Published in final edited form as:
Cell. 2008 October 31; 135(3): 437–448. doi:10.1016/j.cell.2008.08.041.

Nf1-Dependent Tumors Require a Microenvironment Containing *Nf1*$^{+/-}$- and c-kit-Dependent Bone Marrow

Feng-Chun Yang[1,7], **David A. Ingram**[2,7], **Shi Chen**[1,7], **Yuan Zhu**[8,11], **Jin Yuan**[1,7], **Xiaohong Li**[1,7], **Xianlin Yang**[1,7], **Scott Knowles**[1], **Whitney Horn**[1], **Yan Li**[1,7], **Shaobo Zhang**[5], **Yanzhu Yang**[1,7], **Saeed T. Vakili**[5], **Menggang Yu**[6], **Dennis Burns**[9], **Kent Robertson**[1,7], **Gary Hutchins**[3], **Luis F. Parada**[8,10,*], and **D. Wade Clapp**[1,4,7,10,*]

[1]Department of Pediatrics, Indiana University School of Medicine, Indianapolis, IN 46202, USA

[2]Department of Biochemistry and Molecular Biology, Indiana University School of Medicine, Indianapolis, IN 46202, USA

[3]Department of Radiology, Indiana University School of Medicine, Indianapolis, IN 46202, USA

[4]Department of Microbiology and Immunology, Indiana University School of Medicine, Indianapolis, IN 46202, USA

[5]Department of Pathology and Laboratory Medicine, Indiana University School of Medicine, Indianapolis, IN 46202, USA

[6]Department of Biostatistics, Indiana University School of Medicine, Indianapolis, IN 46202, USA

[7]Herman B. Wells Center for Pediatric Research, Indiana University School of Medicine, Indianapolis, IN 46202, USA

[8]Department of Developmental Biology, University of Texas Southwestern Medical Center, Dallas, TX 75390, USA

[9]Department of Pathology, University of Texas Southwestern Medical Center, Dallas, TX 75390, USA

SUMMARY

Interactions between tumorigenic cells and their surrounding microenvironment are critical for tumor progression yet remain incompletely understood. Germline mutations in the *NF1* tumor suppressor gene cause neurofibromatosis type 1 (NF1), a common genetic disorder characterized by complex tumors called neurofibromas. Genetic studies indicate that biallelic loss of *Nf1* is required in the tumorigenic cell of origin in the embryonic Schwann cell lineage. However, in the physiologic state, Schwann cell loss of heterozygosity is not sufficient for neurofibroma formation and *Nf1* haploinsufficiency in at least one additional nonneoplastic lineage is required for tumor progression. Here, we establish that *Nf1* heterozygosity of bone marrow-derived cells in the tumor microenvironment is sufficient to allow neurofibroma progression in the context of Schwann cell *Nf1* deficiency. Further, genetic or pharmacologic attenuation of c-kit signaling in *Nf1*$^{+/-}$

*Correspondence: dclapp@iupui.edu (D.W.C.), luis.parada@utsouthwestern.edu (L.F.P.).
[10]These authors contributed equally to this work.
[11]Current Address: Division of Molecular Medicine and Genetics, University of Michigan Medical School, Ann Arbor, MI 48109

SUPPLEMENTAL DATA

Supplemental Data include seven figures and one table and can be found with this article online at http://www.cell.com/supplemental/S0092-8674(08)01130-6.

hematopoietic cells diminishes neurofibroma initiation and progression. Finally, these studies implicate mast cells as critical mediators of tumor initiation.

INTRODUCTION

Mutations in the *NF1* tumor suppressor gene cause neurofibromatosis type 1 (NF1), a common, pandemic human genetic disorder that affects approximately 250,000 patients in the US, Europe, and Japan alone. The *NF1* gene encodes neurofibromin, a 320 kilodalton protein that functions at least in part as a GTPase-activating protein (GAP) for $p21^{ras}$ (Viskochil et al., 1990; Wallace et al., 1990). The *NF1* cDNA is highly conserved among vertebrate species, with considerable homology extending to yeast and *Drosophila* (Bollag and McCormick, 1991; Martin et al., 1990).

Individuals with NF1 have a wide range of malignant and non-malignant manifestations, including plexiform neurofibromas that collectively affect 25%–40% of NF1 patients and are a major source of lifelong morbidity and mortality. Neurofibromas form in association with peripheral nerves and are composed of Schwann cells, endothelial cells, fibroblasts, degranulating inflammatory mast cells, and pericytes/vascular smooth muscle cells (VSMCs) and contain large collagen deposits. Using an *Nf1* conditional knockout mouse model, we have confirmed retrospective studies from human tumors and demonstrated that *Nf1* loss of heterozygosity (LOH) in the Schwann cell lineage is necessary but not sufficient to elicit neurofibromas (Zhu et al., 2002). In addition, we have reported that tumor progression requires complex interactions between Schwann cells and *Nf1* heterozygous ($Nf1^{+/-}$) cell lineages in the tumor microenvironment (Zhu et al., 2002). Thus, in an *Nf1* wild-type (WT) background, *Nf1* deficiency ($Nf1^{-/-}$ in Schwann cells is necessary but not sufficient to cause tumor formation. A hallmark of the tumor forming heterozygous mice is the appearance of mast cells in peripheral nerves well in advance of tumor development (Zhu et al., 2002). In addition, in vitro experiments mixing conditioned media from Schwann cells and mast cells have demonstrated a hypersensitivity of *Nf1* heterozygous mast cells to conditioned media from *Nf1*-deficient Schwann cells (Yang et al., 2003). Taken together these preceding studies have provided the basis for a model that *Nf1* heterozygous mast cell infiltration of preneoplastic peripheral nerves and association with *Nf1*-deficient Schwann cells is critical for tumor development.

In the present study, we validate the role of NF1 heterozygous bone marrow-derived cells in plexiform neurofibroma formation. Further, on the basis that c-kit receptor activation controls the release of mast cells from the bone marrow, we use both pharmacologic and genetic inhibition of this receptor to prevent or delay plexiform neurofibroma formation in *Nf1* mice. These results establish that *Nf1* haploinsufficiency of bone marrow-derived cells and in particular those dependent on activation of the c-kit receptor is required in the tumor microenvironment to allow neurofibroma progression. The data implicate mast cells as active participants in tumor formation and identify therapeutic targets for human phase 1-2 clinical trials.

RESULTS

Transplantation of $Nf1^{+/-}$ Bone Marrow into Recipients with Biallelic Loss of *Nf1* in Schwann Cells Promotes Increased Morbidity and Mortality

To test the hypothesis that heterozygosity of *Nf1* in hematopoietic cells within the tumor microenvironment is responsible for the genetic haploinsufficiency required for neurofibroma formation, we transferred *Nf1* heterozygous bone marrow into lethally irradiated mice harboring two Krox20-Cre transgene ablated *Nf1* alleles in approximately 10% of Schwann

cells (*Krox20;Nf1*$^{flox/flox}$). *Krox20;Nf1*$^{flox/flox}$ mice are functionally WT in all non Schwann cell lineages and no neurofibromas are observed. As a complementary experiment, WT bone marrow cells were transplanted into lethally irradiated mice containing a germline knockout allele of *Nf1* and a floxed allele susceptible to recombination in the Schwann cell lineage as above (*Krox20;Nf1*$^{flox/-}$). *Krox20;Nf1*$^{flox/-}$ mice uniformly develop plexiform neurofibromas as previously described (Zhu et al., 2002). To identify donor cells and their progeny within the recipients, the *Nf1*$^{+/-}$ and WT donors were inter-crossed with a transgenic mouse that expresses EGFP in all bone marrow cells (Okabe et al., 1997). The intercrossed *Nf1*$^{+/-}$ or WT bone marrow that also expresses EGFP was transplanted into recipients following ionizing radiation, and the development of plexiform neurofibromas and mortality associated with these tumors was monitored until one year of age. A schematic of the experimental design is outlined in Figure 1A. Representative histograms of bone marrow cells in stably reconstituted mice showing EGFP fluorescence is shown in Figure 1B.

Six months after transplantation, the functional germline WT (*Krox20;Nf1*$^{flox/flox}$) recipients engrafted with heterozygous *Nf1*$^{+/-}$ bone marrow began to exhibit motor paralysis, weight loss and only 15% of mice survived the entire experimental period (Figures 2A and 2B). This mortality rate largely mirrored that previously observed in the germline heterozygous *Krox20;Nf1*$^{flox/-}$ mice (Figure 2A). In contrast, approximately 90% of *Krox20;Nf1*$^{flox/flox}$ mice reconstituted with WT bone marrow were alive and exhibited no clinical features of plexiform neurofibroma formation (Figure 2A). Critical validation of these data was provided by the converse experiment in which transplantation of WT bone marrow cells into germline *Nf1* heterozygous, *Krox20;Nf1*$^{flox/-}$, mice restored survival comparable to nontumorigenic *Krox20;Nf1*$^{flox/flox}$ mice that contain intact bone marrow (Figure 2A). Necropsy of the brains and spinal cords of the morbid mice revealed that 21 of 22 *Nf1*$^{+/-}$ bone marrow transplant recipients had an increased thickness of the entire spinal cord as compared to the spinal cords of nonsymptomatic mice transplanted with WT bone marrow (Figure 2C). This abnormal morphology resembles the tumorigenic *Krox20;Nf1*$^{flox/-}$ mice. In addition, we observed multiple, discrete tumors arising from the dorsal root ganglia of *Krox20;Nf1*$^{flox/flox}$ mice transplanted with *Nf1*$^{+/-}$ bone marrow and these tumors were particularly prevalent in the sciatic nerves (Figure 2C, panels 3 and 4). Volumetric analysis of the tumors revealed a 3- to 6-fold increase in volume compared to unaffected dorsal root ganglia in mice that did not develop tumors. The large size and anatomic location of the tumors infiltrating the sciatic nerve and lumbosacral plexus likely account for the observed behavioral abnormalities (Figure 2B and Table S1 available with this article online). In sum, these data indicate that presence of *Nf1* heterozygous bone marrow in the context of Schwann cell loss of heterozygosity is sufficient to recapitulate the morbidity and peripheral nerve hyperplasia originally observed in *Krox20;Nf1*$^{flox/-}$ tumorigenic mice.

Nf1$^{+/-}$ Bone Marrow Recipients Develop Plexiform Neurofibromas

Pathologic analysis confirmed the presence of plexiform neurofibromas in 21 of 22 *Nf1* heterozygous bone marrow recipients (Figure 3A). The dorsal root ganglia from *Krox20;Nf1*$^{flox/flox}$ mice transplanted with *Nf1*$^{+/-}$ bone marrow exhibit classic histological features of human plexiform neurofibromas including disruption of normal architecture; wavy Schwann cells and infiltrating cells with hyperchromatic nuclei (Figure 3A, panels 7 and 8); excess collagen deposition (Figure 3B, panels 2 and 3); angiogenesis (Figure 3C, yellow arrowheads); classic ultrastructural abnormalities (Figure S1) and Schwann cell-specific markers (Figure S2). In contrast, the nerves from either *Krox20;Nf1*$^{flox/flox}$ or *Krox20;Nf1*$^{flox/-}$ mice transplanted with WT marrow exhibited normal appearing evenly distributed nuclei throughout sections of the dorsal root ganglia and proximal peripheral nerves (Figure 3A, panels 1, 4–6, 9, and 10). These mice showed no evidence of collagen deposition

(Figure 3B, panels1, 4, and 5), neovascularization, and retained normal ultra-structural morphology (Figure S1).

Neurofibromas Are Infiltrated with Donor Mast Cells

As described above, neurofibromas are complex tumors comprising multiple cell types in which LOH is uniquely present in the Schwann cell lineage (Zhu et al., 2002). Mast cell infiltration is characteristic of human and murine plexiform neurofibromas (Hirota et al., 1993; Zhu et al., 2002). In our mouse model, we observe peripheral nerve infiltration by mast cells preceding tumor appearance. Accordingly, the $Nf1^{+/-}$ bone marrow of reconstituted $Krox20;Nf1^{flox/flox}$ mice also exhibited extensive mast cell infiltration as evidenced by mast cell-specific stains (Figures 3C, panels 2 and 3, 3D, and S3). To further discern the identity of bone marrow-derived lineages in the tumor, fluorescence cytometry was utilized to identify hematopoietic cells (CD45.2+) in the neurofibromas of $Krox20;Nf1^{flox/flox}$ mice transplanted with $Nf1^{+/-}$ bone marrow (Figure 3E). In 12 tumors examined, a range of 3%–7% of the cells were hematopoietic cells (CD45.2+; EGFP+). From this population, the majority of cells were identified as mast cells (CD117+; FcεRI+;EGFP+, Figure 3E, panel 3). A small population of macrophages (Figure 3D, panel 4) and rare B lymphocyte and T-lymphocyte populations were also observed (Figure 3E, panels 4 and 5). Consistent with the histological sections, there were no comparable populations of hematopoietic cells observed in dorsal root ganglia from $Krox20;Nf1^{flox/flox}$ mice transplanted with WT bone marrow (data not shown). Subsequent genotyping confirmed that hematopoietic but not endothelial or fibroblast populations harbored the *Nf1* null allele (Figure 3F). These data confirm the appearance of bona fide plexiform neurofibromas in the reconstituted $Krox20;Nf1^{flox/flox}$ mice including homing of the transplanted heterozygous mast cells to the sites of *Nf1*-deficient Schwann cells. Collectively, the bone marrow transplantation experiments into $Krox20;Nf1^{flox/flox}$ mice demonstrate that in the context of disruption of *Nf1* in the embryonic Schwann cell lineage, $Nf1^{+/-}$ bone marrow is sufficient for tumor progression. Furthermore, the converse experiment of transplanting WT bone marrow into tumor prone $Krox20;Nf1^{flox/-}$ mice demonstrates that in this mouse model, $Nf1^{+/-}$ bone marrow is required for tumor progression.

$Nf1^{+/-}$ Bone Marrow-Mediated Tumor Formation Requires c-kit

The fact that the only $Nf1^{+/-}$ cells detected in the reconstituted plexiform neurofibromas were bone marrow-derived was consistent with our previous in vitro and in vivo observations implicating a mast cell haploinsufficiency requirement in tumor formation (Ingram et al., 2000; Yang et al., 2003; Zhu et al., 2002). The c-kit receptor tyrosine kinase (RTK) controls many aspects of mast cell development and function (Galli et al., 1993). We have reported that c-kit activity governs migration, proliferation, and survival of $Nf1^{+/-}$ bone marrow-derived mast cells (Ingram et al., 2000, 2001; Yang et al., 2003). We therefore next tested whether genetic disruption of c-kit activity in $Nf1^{+/-}$ bone marrow cells transplanted into $Krox20;Nf1^{flox/flox}$ mice would affect tumor progression.

$Nf1^{+/-}$ mice were independently intercrossed with two hypomorphic strains of mice deficient in mast cell mobilization by virtue of point mutations in the c-kit receptor that reduce kinase activity 85% (W^{41}/W^{41}) or 95% (W^{v}/W^{v}), respectively. The bone marrow from either $Nf1^{+/-};W^{v}/W^{v}$ or $Nf1^{+/-};W^{41}/W^{41}$ doubly mutant mice was transplanted into five and ten recipient $Krox20;Nf1^{flox/flox}$ mice respectively that had been previously irradiated with a dosage of ionizing radiation that induces bone marrow failure and lethality in the absence of a donor graft (Haneline et al., 1999). Morbidity of mice engrafted with $Nf1^{+/-};W$ mutant marrow was significantly reduced as compared to $Nf1^{flox/flox}$ mice transplanted with $Nf1^{+/-}$ bone marrow (Figure 4A). Accordingly, in contrast to recipients of $Nf1^{+/-}$ bone marrow, the dorsal root ganglia and proximal peripheral nerves from the $Krox20;Nf1^{flox/flox}$ mice transplanted with $Nf1^{+/-};W$ mutant marrow do not exhibit gross evidence of tumors (Figures 4A–4C).

Furthermore, they do not exhibit histological features of neurofibromas (Figure 4D) nor evidence of invading hematopoietic cells as measured by fluorescence cytometry (data not shown).

Despite the fact that recipient mice are lethally irradiated prior to bone marrow transplant, it is well known that W mutant bone marrow can be competitively overcome by wild-type bone marrow in vivo. Because of the complexity of intercrossing multiple alleles and infertility of the W^v/W^v mice, it was not possible to intercross the EGFP allele onto the intercrossed *Nf1*$^{+/-}$;*W* mutant line. Therefore to rule out the possibility of any residual wild-type (*Nf1*$^{flox/flox}$) recipient bone marrow overcoming the donor *Nf1*$^{+/-}$;*W* bone marrow, we verified the predominant presence of the donor heterozygous genotype in bone marrow derivatives of engrafted animals (Clapp et al., 1995; Jordan et al., 1990). Southern blot analysis of bone marrow from five randomly selected *Nf1*$^{flox/flox}$;*Krox20-cre* recipients demonstrated predominant (>85%–100%) presence of the *Nf1*$^{+/-}$ genotype indicating effective donor engraftment of heterozygous bone marrow (Figure S4A). In addition, DNA from forty individual granulocyte macrophage and mast cell progenitors from each recipient, which grow as individual colonies in semisolid medium, was examined for detection of the *Nf1* knockout, WT and Cre/lox alleles (Figure S4B). Approximately 95% of all progenitors examined (193/200) contained the *Nf1* knockout allele but not the *Nf1*$^{flox/flox}$ allele. Collectively, these molecular data demonstrate the effective engraftment of donor marrow and further refine the identity of the active component of the *Nf1*$^{+/-}$ marrow to a c-kit dependent cell type.

Pharmacologic Inhibition of c-kit Reduces Tumor Size and Metabolic Activity

The availability of pharmacologic agents that can inhibit c-kit receptor activity permitted us to next examine whether such agents could affect neurofibroma formation or persistence. Imatinib mesylate is a potent inhibitor of the c-kit, PDGFR, and c-abl tyrosine kinases. To assess the activity of imatinib mesylate and other potential pharmacologic agents on tumor burden we validated a noninvasive fluoridinated deoxyglucose positron emission tomography (FDG-PET) imaging protocol permitting identification and longitudinal observation of plexiform neurofibromas in *Krox20;Nf1*$^{flox/-}$ mice (see Experimental Procedures and Figures S5A–S5C).

We next selected cohorts of 8- to 9-month-old *Krox20;Nf1*$^{flox/-}$ mice with confirmed PET positive uptake in the region of the sciatic nerve for oral treatment with either 200 mg/kg/day of imatinib mesylate or a placebo control (PBS). FDG-PET imaging studies followed to evaluate the evolution of the tumors. Representative FDG-PET axial slices of affected nerves from three mice imaged before and after treatment with imatinib mesylate or PBS for 3 weeks are shown in Figure 5A. As predicted, increased FDG uptake was seen in *Krox20*;*Nf1*$^{flox/-}$ animals lateral to the spine prior to treatment with either imatinib mesylate or PBS (Figure 5A, panels 1, 3, and 5). Strikingly, FDG uptake was qualitatively reduced in the *Krox20;Nf1*$^{flox/-}$ mice treated with imatinib mesylate (Figure 5A, panels 2–4) compared to the PBS controls (Figure 5A, panel 6). To carefully measure the FDG-PET intensity in all treated animals, a standardized region of interest (ROI) was utilized in each animal to extract quantitative FDG uptake values (mCi/ml tissue). Three dimensional ROIs in the shape of cylinders were utilized to encapsulate the areas lateral to the spinal column with the ROI cylinders and specific vertebrae landmarks (lumbar 1-sacral 1) were used in all cases to assure consistency. Representative results from one experimental animal, before and after treatment, are shown in panels 7 and 8 (Figure 5A). A summary of these results for the sciatic nerve region ROIs of one cohort of 12 experimental mice are plotted in Figure 5B. Overall, the mice treated with imatinib mesylate had a mean 50% reduction in FDG-PET uptake after treatment ($p < 0.035$). In contrast, the metabolic activity of the tumors in the cohort treated with PBS had a modest but not significant increase in the FDG uptake ratio comparable to the progressive

uptake in FDG observed as a function of time in emerging plexiform neurofibromas in *Krox20;Nf1*$^{flox/-}$ mice.

To determine whether a change in metabolic activity (FDG uptake) directly correlated with histological changes in the tumors, the imaged cohorts were sacrificed, the spinal cords were examined, and sections were prepared for histologic evaluation. At postmortem, we also compared the volumes of all dorsal root ganglia from an age equivalent cohort of *Krox20;Nf1*$^{flox/flox}$ mice. Consistent with the FDG-PET imaging studies, there was a clear decrease in dorsal root ganglia volume in the imatinib mesylate treated group as compared to the PBS treated group (Figure 5C).

Histological evaluation of the dorsal root ganglia and proximal surrounding nerves in mice treated with either imatinib mesylate or PBS was also conducted. Nerves harvested from placebo treated mice showed a distinct disruption of the normal nerve architecture and an increase in cellularity compared to imatinib mesylate treated mice. This is illustrated in tissue sections showing the distal dorsal root and proximal nerve segments (Figure 5D, panels1–6 compared to 7–12). Further, there is a marked reduction in the number of mast cells in nerves dissected from mice treated with imatinib mesylate compared to PBS treated controls (Figure 5D, panels 3 and 4 versus 9 and 10, Figure 5E). This reduction in tumor size is also associated with both an increase in apoptotic cells within the tumor (Figures 5F and S6) and a decrease in proliferation (Figure 5G). Collectively, the PET, gross anatomic and histological data identify the potential for imatinib mesylate to reduce tumor volume in *Krox20;Nf1*$^{flox/-}$ mice.

Imatinib Mesylate Treatment Reduces Plexiform Neurofibroma Size and Associated Symptoms

Plexiform neurofibromas primarily present in infants and young children with NF1 and are frequently characterized by rapid growth and invasion into adjacent organs often resulting in impairment of normal organ function. These tumors can be life threatening and present major clinical challenges as surgical treatment has limited effectiveness, and no alternative therapies are currently available. As the present murine studies were nearing conclusion, a three year-old child with classic stigmata of NF1 including a plexiform neurofibroma presented with progressive life threatening airway compression. The tumor was originally diagnosed at age 6 months when a slow progressively enlarging mass of the left floor of the mouth, tongue, neck, and mastoid bone with encasement of the carotid artery and jugular vein was biopsied and histologically confirmed to be a neurofibroma. The tumor was deemed unresectable given the vascular involvement and she was observed clinically with sequential magnetic resonance imaging (MRI) scans. Over the next 2 years, the tumor progressed to cause upper airway compression (Figure 6) manifested by difficulty sleeping, poor appetite, and episodes of drooling. A sleep study showed frequent interruptions of sleep but no oxygen desaturations to less than 91%. Based on these findings, the attending physician placed the child on 350 mg/m^2/dose of imatinib mesylate for a limited trial. The parents provided consent for the use of imatinib mesylate following discussion of the recent research results at our institutions, potential risks and benefits of imatinib mesylate, and acknowledgment that although imatinib mesylate was a widely used drug for leukemias and solid tumors, including uses in infants, there was no human data for imatinib mesylate in NF1 related tumors. MRI scans before and after three months of treatment revealed a remarkable approximately 70% reduction in tumor volume (Figures 6 and S7). Following treatment for six months with no observed side effects (NCI CTC version 3 toxicity scale, http://ctep.cancer.gov), MRI scans showed stabilization of her response (Figure S7) without further reduction and the patient came off treatment. Though reflecting the course of a single patient, this striking result is consistent with the preclinical studies in the murine model.

DISCUSSION

Theories concerning the cellular and molecular mechanisms that underlie the development of idiopathic cancer have undergone significant evolution in recent years. The original notions that cell autonomous events convey a single cell to overcome its normal regulation leading to development of malignant disease, and furthermore the identity of the cell type of tumor origin, are presently under concerted reinvestigation. It is increasingly clear that while a series of genetic and epigenetic events in a single cell commence the trajectory toward a malignant phenotype, most forms of cancer include a cooption of a permissive microenvironment that allows and even promotes the tumorigenic state (Hanahan and Weinberg, 2000). Following this hypothesis, a resistant environment would essentially preclude the possibility of tumor formation. Among identified noncell autonomous contributors to a coopted permissive process of tumor formation are neoangiogenesis, participation of the local stroma, and inflammation, among other cell types (Bhowmick et al., 2004; Coussens and Werb, 2002). The understanding of the precise order of paracrine interactions, the relative importance, and the molecular basis of the nontumorigenic environment interaction, remains in infancy.

In this context, the development of murine mouse models that might permit dissection of cell autonomous and noncell autonomous contributions to tumor development has gained considerable ascendance. Mouse tumor models clearly require rigorous scrutiny in that the significance of such experimental strategies can only be appreciated in the context of a clear and verifiable physiological relevance to the human status. Therefore, a cardinal principle in mouse modeling of human cancer requires that mutations of relevant molecular pathways be developed in the same tissues as the human tumors. Further, the mouse tumors should recapitulate the human phenotype in a credible series of cellular and molecular outcomes.

Neurofibromatosis type 1 is a single gene disease that in the vast majority of cases is manifested by germline mutation and therefore complete somatic heterozygosity followed by rare loss of heterozygosity in cell types that engender the stereotypic manifestations of this disease. Invariably tumors develop in the peripheral nervous system. Human tissue studies suggested a critical role for Schwann cells but suffered from relying on a posteriori information to infer a preceding event. A conditional *Nf1* knockout mouse model that permitted tissue-specific deletion of *Nf1* has shed light on this process. In the physiologically relevant context of global heterozygosity, these studies revealed the genetic bottleneck for plexiform neurofibroma formation to lie in the loss of *Nf1* heterozygosity in the embryonic Schwann cell lineage (Zhu et al., 2002). The histopathological analysis of these tumors was indistinguishable from native human tumors.

The Microenvironment and Plexiform Neurofibromas

The power of mouse genetics further revealed a critical role for a microenvironment that could in distinct genetic configurations, be either tumor permissive or tumor resistant. Two key observations prompted the idea that mast cells were strong candidates to be critical participants in plexiform neurofibroma initiation (Zhu et al., 2002). First was the realization that *Nf1* heterozygosity outside the Schwann cell lineage was required for tumor formation. Next, was the observation that mast cell infiltration into peripheral nerves appeared in these mice months prior to tumor appearance, but not in the non tumorigenic *Nf1* wild-type (*flox/flox*) genotype. Mast cells have been observed in human neurofibromas although in the absence of a mouse model, examination of a functional role in tumor development or maintenance could not be directly studied. The requirement for *Nf1* haploinsufficiency has been replicated with additional Cre transgenes that target the neural crest Schwann cell lineage including periostin-Cre, P0-Cre and tamoxifen inducible PLP-Cre, thus further validating the need for *Nf1* heterozygosity outside the Schwann cell lineage (our unpublished data). The original and now additional confirmatory data using tissue-specific Cre transgenes do not preclude that tumors

might be achievable in a wild-type environment under contrived experimental conditions. Indeed, when we utilize neural crest-specific Cre drivers that have early, widespread, and robust expression, thus driving *Nf1* nullizygosity throughout neural crest-derived cells, we observe hyperplasia of the peripheral nerves even in *flox/flox* mice, although less so than in the *flox/−* condition (unpublished data). We believe these latter models depart from the physiological situation in humans with NF1 wherein LOH is a rare stochastic event. In human patients with NF1, a rare embryonic LOH event renders a Schwann $Nf1^{-/-}$ cell in isolation and at relative disadvantage within its microenvironment to mount tumor formation as compared to experimental supraphysiologic disruption in broad fields of $Nf1^{-/-}$ Schwann cells. Our mouse models indicate that an isolated $Nf1^{-/-}$ pocket of Schwann cells gains a significant selective advantage by an evident synergy with recruited heterozygous mast cells. We interpret the hyperplasia in robust Cre embryonic mediated recombination models to reflect a nonphysiologic widespread loss of *Nf1*, not only in most Schwann cells but also in additional neural crest lineages that may help to partially overcome the barriers of isolated LOH.

Nf1 Heterozygous Mast Cells Require c-kit for Tumor Formation and Maintenance

The finding that transplantation of WT bone marrow into tumor prone $Krox20;Nf1^{flox/-}$ mice rescues tumorigenicity establishes that the requirement for haploinsufficiency resides in bone marrow-derived cells but not other cell types found in these tumors. Conversely, genetic disruption of c-kit signaling in the donor bone marrow, resulting in failure of donor heterozygous mast cells to infiltrate peripheral nerves and absence of tumors strongly supports the hypothesis that this constitutes a causal interaction.

The c-kit receptor has a central role in mast cell development and function (Huang et al., 1990). Schwann cells and fibroblasts, two principal components of neurofibromas, secrete kit-ligand in response to many different stimuli (Hirota et al., 1993; Ryan et al., 1994). Elevated kit-ligand mRNA transcripts have been reported in neurofibroma tissue and it has been reported that NF1 patients have elevated levels of kit ligand in serum (Mashour et al., 2004). We therefore turned to imatinib mesylate, an FDA-approved pharmacological agent that has inhibitory activity on several tyrosine kinases including c-kit in preclinical trials. In tissue culture studies, we found that the ability of conditioned media from $Nf1^{-/-}$ Schwann cells to hyper stimulate proliferation of cultured heterozygous ($Nf1^{+/-}$) mast cells is essentially blocked by imatinib mesylate (data not shown; Yang et al., 2003). We were surprised by the dramatic activity of this drug to reverse the neurofibroma pathology in our mouse model accompanied by disappearance of mast cells from the peripheral nerves. In addition to extending our in vitro studies that demonstrated c-kit mediated interactions between $Nf1^{-/-}$ Schwann cells and heterozygous mast cells (Yang et al., 2003), the in vivo studies identify a persisting requirement for imatinib mesylate-susceptible cells for tumor maintenance. Whether sustained treatment is required after tumor regression awaits further investigation.

The role of inflammatory cells in tumor development is an active area of research (Coussens et al., 1999, 2000; Coussens and Werb, 2002). It is now evident that inflammatory cells are critical to the early genesis of evolving neoplasms and it is implicated in a wide range of murine tumorigenesis models, including breast, ovarian (Kacinski, 1995), pancreatic (Bergers et al., 2000), and skin models (Coussens et al., 1999). The presence of mast cells in neurofibromas is an old and accepted observation that has led to speculation about a potential active role in tumor development or maintenance. Mast cells have also been implicated in other skin malignancies in both human and murine systems (Coussens et al., 1999; Galli et al., 1993; Hirota et al., 1993; Ryan et al., 1994).

Mast cells release mediators of inflammation including histamine, serotonin, proteoglycans, and leukotrienes subsequent to activation of the high affinity IgE receptor (FcεRI) and the c-kit receptor (Galli et al., 1993; Boesiger et al., 1998). Further, mast cells release VEGF

(Boesiger et al., 1998), an angiogenic factor that is also a potent proliferative, survival, and chemotactic factor for Schwann cells (Sondell et al., 1999). VEGF has also been linked to an angiogenic switch in tumor formation (Bergers et al., 2000). Finally, mast cells also release PDGF-BB, a growth factor that promotes pericyte and fibroblast proliferation; and TGF-β, a growth factor that promotes fibroblast proliferation and collagen synthesis.

Imatinib Mesylate and the Tumor Microenvironment

In the context of neurofibromas, how do mast cells cooperate with Schwann cells to elicit tumor formation? We show that other cell types in the tumor needn't have NF1 mutations. However, we cannot at this time assert whether the infiltrating *Nf1* heterozygous mast cell primarily acts reciprocally on the *Nf1*-deficient Schwann cells to promote tumor formation or alternatively whether indirect interaction with local stroma and additional cell types also present in these tumors are requisite intermediaries for tumor induction. Studies are underway to gain a better understanding of additional paracrine interactions within neurofibromas and how they may impinge on tumor formation and maintenance. In addition to the above genetic results, our previous in vitro studies demonstrated that imatinib mesylate inhibits multiple $Nf1^{+/-}$ pericyte, and fibroblast tumor promoting functions (Li et al., 2006; Munchhof et al., 2006; Yang et al., 2006). Again, despite the absence of requirement for heterozygosity in these additional tumor cells, we cannot rule out that the activity of imatinib mesylate in regressing tumors may extend beyond its inhibitory activity on mast cells. Imatinib mesylate could in principle fortuitously inhibit additional potentially critical tumor promoting activities of other cell types. For instance in addition to inhibiting c-kit in mast cells, imatinib mesylate may decrease angiogenesis by blocking PDGF receptor and/or reduce fibrosis/collagen production by blocking c-abl. Additional investigation will be required to resolve these critical and fascinating scenarios.

A critically ill three year-old child with a plexiform neurofibroma compressing her airway was administered imatinib mesylate therapy in a compassionate use protocol and responded dramatically to this therapy. This encouraging and coincident result together with results obtained from our mouse model has prompted a Phase 2 clinical trial to determine the efficacy of this treatment for plexiform neurofibromas. One cautionary note concerns the limitation that our mouse model has a relatively short lifespan. On the basis of one-year mouse tumor studies, we cannot predict with certainty how long-lived tumors might be expected to respond to imatinib mesylate. It is also conceivable that long lived tumor cells in NF1 patients may accrue additional properties over time that render them independent of certain early paracrine events such as the mast/Schwann cell nexus.

Conclusions

The present studies provide an example of a physiologically relevant mouse model of a human cancer that has provided concrete insights into complex interactions between the tumor cell of origin and the microenvironment. On the basis of these studies, we have developed a potential therapeutic approach for a heretofore untreatable tumor by targeting the microenvironment rather than the tumorigenic cell. Should the activity of imatinib mesylate prove to be validated in clinical trials, unlike the situation with this drug in treatment of chronic myelogenous leukemia, we would not anticipate the eventual development of drug resistance. In CML, the action of imatinib mesylate is directly on the leukemic cell and aimed at a mutated constitutively active tyrosine kinase oncoprotein (Bcr-abl). The Bcr-abl oncogene can develop drug resistance through acquisition of second site mutations (Sawyers, 2005). In contrast, we believe that the principal if not exclusive activity of imatinib mesylate on neurofibromas is on non tumor cells acting on wild-type proteins for which there is presumably no pressure for selection for drug resistance. Currently, we have identified compounds that in vitro have as much as tenfold higher inhibitory activity on *Nf1* heterozygous mast cells than does imatinib mesylate (unpublished data). Preclinical tests will help determine whether these compounds will exhibit

increased potential for therapeutic avenues in NF1. It is interesting to note that extremely rare patients have been reported that have both neurofibromatosis type 1 and piebaldism, a rare neural crest disease that affects pigmentation and the enteric nervous system. Although not directly evaluated, based on independent studies on the molecular basis of piebaldism, the authors of these studies inferred, that piebaldism presumably resulted from hypomorphic mutations of the c-kit receptor. Remarkably, these patients were reported to lack neurofibromas (Chang et al., 1993; Tay, 1998). In retrospect, it is highly likely that these NF1/piebald patients were deficient in mast cells thus providing a human confirmation of the importance of c-kit and mast cells in neurofibroma formation. In closing we suggest that the genetic and cellular malleability of our neurofibroma mouse model may reveal important details about microenvironment participation and paracrine cell interactions in tumor formation that will have general relevance for human cancer outside the context of neurofibromatosis type 1.

EXPERIMENTAL PROCEDURES

Animals and Reagents

The *Krox20;Nf1*$^{flox/flox}$ mice and *Krox20;Nf1*$^{flox/-}$ mice have been previously described (Zhu et al., 2002). The C57BL/6-TgN(ACTbEGFP)1Osb mice were obtained from Jackson Laboratory, Bar Harbor, ME. Chemicals were purchased from Sigma (St. Louis, MO) unless otherwise stated.

Bone Marrow Transplantation of Hematopoietic Cells

Two million syngeneic WT or *Nf1*$^{+/-}$ bone marrow cells from WT GFP or *Nf1*$^{+/-}$ GFP mice per recipient were transplanted into young adult *Krox20;Nf1*$^{flox/flox}$ mice or *Krox20;Nf1*$^{flox/-}$ mice following 1100 rads of ionizing radiation.

PET Imaging Analysis

Fluorodeoxyglucose ([^{18}F] FDG) PET and X-ray CT imaging was employed to identify neurofibromas. CT images were used to place a standardized volume of interest (VOI) template over regions lateral to the spinal cord for quantification of FDG uptake. Registered and overlaid CT image data was used to identify specific vertebrae landmarks from Lumbar (L1) to the Sacrum (S1). The user then picked points along the spinal cord to determine the path of the spinal cord between L1 and S1. Three circular regions-of-interest (ROI) are then placed at interpolated points along the spinal cord to capture the spinal cord and the dorsal root ganglion regions. The circular ROI's then were combined to create VOI's for the spinal cord, left dorsal root ganglion, and right dorsal root ganglion. FDG images were acquired at 45 min postinjection of 0.5–1.0 mCi of FDG via tail vein injection. All animals were administered FDG while awake and given isoflurane anesthesia at 40 min postinjection to immobilize the animal for imaging.

Dissection of Dorsal Root Ganglia

Immediately following postmortem, mice were perfused and fixed in 4% paraformaldehyde. The dorsal root ganglia and peripheral nerves were then dissected out under a dissection microscope.

Measurement of Tumor Size

The volume of tumors was determined by the established approximate volume for a spheroid $0.52 \times (\text{width})^2 \times \text{length}$.

Phenotypic Evaluation of the Donor Cells in Dorsal Root Ganglia

Ganglia were minced, digested by collagenase V, and the single cell suspension was admixed with anti CD117, CD31, or Col1A and FcεRI antibodies. Populations were separated using a fluorescence-activated cell sorter (Becton Dickson, San Jose, CA).

Genotypic Analysis of Donor Bone Marrow

DNA was isolated as described (Clapp et al., 1995), digested with PstI to elucidate the *Nf1* knockout and $Nf1^{flox/flox}$ fragments and separated by gel electrophoresis. Following transfer to a nitrocellulose filter, fragments were hybridized with an Eag I/ Sph I, ^{32}P dATP labeled *neo* fragment, washed, and exposed to film as described (Clapp et al., 1995).

Histological Analysis

To examine the morphology of the tumors in detail, paraffin sections were stained with hematoxylin and eosin (H&E), masson trichrome alcian blue as described (Zhu et al., 2002).

In Vivo Evaluation of Proliferation and Survival in Tumors

Cell proliferation in tumors was evaluated by utilizing a BrdU in situ detection kit (BD PharMingen, San Jose, CA). *Krox20;*$Nf1^{flox/-}$ mice previously treated for 12 weeks with imatinib or vehicle, received 50 mg BrdU per Kg of body weight), 48, 24, 6, 4, and 2 hr via peritoneal injection before intracardiac perfusion. DRGs were processed for paraffin-embedding immunohistochemical staining and BrdU positive cells were counted under a phase contrast microscope. Apoptosis of tissues was evaluated using TUNEL staining as described (Hiatt et al., 2004).

Transmission Electron Microscopy

Following perfusion fixation, tissues were dehydrated in a graded series of ethanol and acetone and embedded in Epon-Araldite (Electron Microscopy Sciences, Hatfield, PA). Ultrathin sections (silver to gold) were stained with uranyl acetate and lead citrate and examined with a FEI Tecnai G2 electron microscope (Philips, Eindhoven, Netherlands).

Statistical Methods

Analysis of survival outcomes was performed using the Kaplan-Meier method. Comparison of the mean size of tumors, differences in cellularity and apoptosis in the experimental groups was performed using Student's t test or analysis of variance.

Supplementary Material

Refer to Web version on PubMed Central for supplementary material.

Acknowledgments

This work was supported by the Department of Defense (NF020026) to D.W.C. and L.F.P., a P50 Center of Excellence in Neurofibromatosis P50 NS 052606 (L.F.P., D.W.C., F.C.Y., D.A.I., and G.H.) and R01 CA74177 to D.W.C. L.F.P. is an American Cancer Society Professor and also acknowledges support from the NCI-MMHC. Novartis supplied imatinib mesylate to D.W.C. for these studies. The work was also supported by the Anna Fuller Foundation.

REFERENCES

Bergers G, Brekken R, McMahon G, Vu TH, Itoh T, Tamaki K, Tanzawa K, Thorpe P, Itohara S, Werb Z, Hanahan D. Matrix metalloproteinase-9 triggers the angiogenic switch during carcinogenesis. Nat. Cell Biol 2000;2:737–744. [PubMed: 11025665]

Bhowmick NA, Chytil A, Plieth D, Gorska AE, Dumont N, Shappell S, Washington MK, Neilson EG, Moses HL. TGF-beta signaling in fibroblasts modulates the oncogenic potential of adjacent epithelia. Science 2004;303:848–851. [PubMed: 14764882]

Boesiger J, Tsai M, Maurer M, Yamaguchi M, Brown LF, Claffey KP, Dvorak HF, Galli SJ. Mast cells can secrete vascular permeability factor/ vascular endothelial cell growth factor and exhibit enhanced release after immunoglobulin E-dependent upregulation of fc epsilon receptor I expression. J. Exp. Med 1998;188:1135–1145. [PubMed: 9743532]

Bollag G, McCormick F. Differential regulation of rasGAP and neurofibromatosis gene product activities. Nature 1991;351:576–579. [PubMed: 1904555]

Chang T, McGrae JD Jr. Hashimoto K. Ultrastructural study of two patients with both piebaldism and neurofibromatosis 1. Pediatr. Dermatol 1993;10:224–234. [PubMed: 8415298]

Clapp DW, Freie B, Lee WH, Zhang YY. Molecular evidence that in situ-transduced fetal liver hematopoietic stem/progenitor cells give rise to medullary hematopoiesis in adult rats. Blood 1995;86:2113–2122. [PubMed: 7662959]

Coussens LM, Raymond WW, Bergers G, Laig-Webster M, Behrendtsen O, Werb Z, Caughey GH, Hanahan D. Inflammatory mast cells up-regulate angiogenesis during squamous epithelial carcinogenesis. Genes Dev 1999;13:1382–1397. [PubMed: 10364156]

Coussens LM, Tinkle CL, Hanahan D, Werb Z. MMP-9 supplied by bone marrow-derived cells contributes to skin carcinogenesis. Cell 2000;103:481–490. [PubMed: 11081634]

Coussens LM, Werb Z. Inflammation and cancer. Nature 2002;420:860–867. [PubMed: 12490959]

Galli SJ, Tsai M, Wershil BK. The c-kit receptor, stem cell factor, and mast cells. Am. J. Pathol 1993;142:965–974. [PubMed: 7682764]

Hanahan D, Weinberg RA. The hallmarks of cancer. Cell 2000;100:57–70. [PubMed: 10647931]

Haneline LS, Gobbett TA, Ramani R, Carreau M, Buchwald M, Yoder MC, Clapp DW. Loss of *Fanc*C function results in decreased hematopoietic stem cell repopulating ability. Blood 1999;94:1–8. [PubMed: 10381491]

Hiatt K, Ingram DA, Huddleston H, Spandau DF, Kapur R, Clapp DW. Loss of the *Nf1* tumor suppressor gene decreases Fas antgen expression in myeloid cells. Am. J. Pathol 2004;164:1471–1479. [PubMed: 15039234]

Hirota S, Nomura S, Asada H, Ito A, Morii E, Kitamura Y. Possible involvement of c-kit Receptor and its ligand in increase of mast cells in neurofibroma tissues. Arch. Pathol. Lab. Med 1993;117:996–999. [PubMed: 7692836]

Huang E, Nocka K, Beier DR, Chu TY, Buck J, Lahm HW, Wellner D, Leder P, Besmer P. The hematopoietic growth factor KL is encoded by the Sl locus and is the ligand of the c-kit receptor, the gene product of the W locus. Cell 1990;63:225–233. [PubMed: 1698557]

Ingram DA, Yang FC, Travers JB, Wenning MJ, Hiatt K, New S, Hood A, Shannon K, Williams DA, Clapp DW. Genetic and biochemical evidence that haploinsufficiency of the *Nf1* tumor suppressor gene modulates melanocyte and mast cell fates in vivo. J. Exp. Med 2000;191:181–188. [PubMed: 10620616]

Ingram DA, Hiatt K, King AJ, Fisher L, Shivakumar R, Derstine C, Wenning MJ, Diaz B, Travers JB, Hood A, et al. Hyperactivation of p21ras and the hematopoietic-specific Rho GTPase, Rac2, cooperate to alter the proliferation of neurofibromin deficient mast cells in vivo and in vitro. J. Exp. Med 2001;194:57–69. [PubMed: 11435472]

Jordan CT, McKearn JP, Lemischka IR. Cellular and developmental properties of fetal hematopoietic stem cells. Cell 1990;61:953–963. [PubMed: 1972037]

Kacinski BM. CSF-1 and its receptor in ovarian, endometrial and breast cancer. Ann. Med 1995;27:79–85. [PubMed: 7742005]

Li F, Munchhof AM, White HA, Mead LE, Krier TR, Fenoglio A, Chen S, Wu X, Cai S, Yang FC, Ingram DA. Neurofibromin is a novel regulator of RAS-induced signals in primary vascular smooth muscle cells. Hum. Mol. Genet 2006;15:1921–1930. [PubMed: 16644864]

Martin GA, Viskochil D, Bollag G, McCabe PC, Crosier WJ, Haubruck H, Conroy L, Clark R, O'Connell P, Cawthon RM, et al. The GAP-related domain of the neurofibromatosis type 1 gene product interacts with ras p21. Cell 1990;63:843–849. [PubMed: 2121370]

Mashour GA, Driever PH, Hartmann M, Drissel SN, Zhang T, Scharf B, Felderhoff-Muser U, Sakuma S, Friedrich RE, Martuza RL, et al. Circulating growth factor levels are associated with tumorigenesis in neurofibromatosis type 1. Clin. Cancer Res 2004;10:5677–5683. [PubMed: 15355893]

Munchhof AM, Li F, White HA, Mead LE, Krier TR, Fenoglio A, Li X, Yuan J, Yang FC, Ingram DA. Neurofibroma-associated growth factors activate a distinct signaling network to alter the function of neurofibromin-deficient endothelial cells. Hum. Mol. Genet 2006;15:1858–1869. [PubMed: 16648142]

Okabe M, Ikawa M, Kominami K, Nakanishi T, Nishimune Y. 'Green mice' as a source of ubiquitous green cells. FEBS Lett 1997;407:313–319. [PubMed: 9175875]

Ryan JJ, Klein KA, Neuberger TJ, Leftwich JA, Westin EH, Kauma S, Fletcher JA, DeVries GH, Huff TF. Role for the stem cell factor/ KIT complex in Schwann cell neoplasia and mast cell proliferation associated with neurofibromatosis. J. Neurosci. Res 1994;37:415–432. [PubMed: 7513766]

Sawyers CL. Making progress through molecular attacks on cancer. Cold Spring Harb. Symp. Quant. Biol 2005;70:479–482. [PubMed: 16869786]

Sondell M, Lundborg G, Kanje M. Vascular endothelial growth factor has neurotrophic activity and stimulates axonal outgrowth, enhancing cell survival and Schwann cell proliferation in the peripheral nervous system. J. Neurosci 1999;19:5731–5740. [PubMed: 10407014]

Tay YK. Neurofibromatosis 1 and Piebaldism: A case report. Dermatology 1998;197:401–402. [PubMed: 9873189]

Viskochil D, Buchberg AM, Xu G, Cawthon RM, Stevens J, Wolff RK, Culver M, Carey JC, Copeland NG, Jenkins NA. Deletions and a translocation interrupt a cloned gene at the neurofibromatosis type 1 locus. Cell 1990;62:187–192. [PubMed: 1694727]

Wallace MR, Marchuk DA, Andersen LB, Letcher R, Odeh HM, Saulino AM, Fountain JW, Brereton A, Nicholson J, Mitchell AL. Type 1 neurofibromatosis gene: identification of a large transcript disrupted in three NF1 patients. Science 1990;249:181–186. [PubMed: 2134734]

Yang FC, Chen S, Clegg T, Li X, Morgan T, Estwick SA, Yuan J, Khalaf W, Burgin S, Travers J, et al. Nf1+/− mast cells induce neurofibroma like phenotypes through secreted TGF-beta signaling. Hum. Mol. Genet 2006;15:2421–2437. [PubMed: 16835260]

Yang FC, Ingram DA, Chen S, Li X, Clegg TE, White H, Mead L, Atkinson S, Kapur R, Williams DA, Clapp DW. Neurofibromin-deficient Schwann cells secrete a potent migratory stimulus for *Nf1* +/− mast cells. J. Clin. Invest 2003;112:1851–1861. [PubMed: 14679180]

Zhu Y, Ghosh P, Charnay P, Burns DK, Parada LF. Neurofibromas in NF1: Schwann cell origin and role of tumor environment. Science 2002;296:920–922. [PubMed: 11988578]

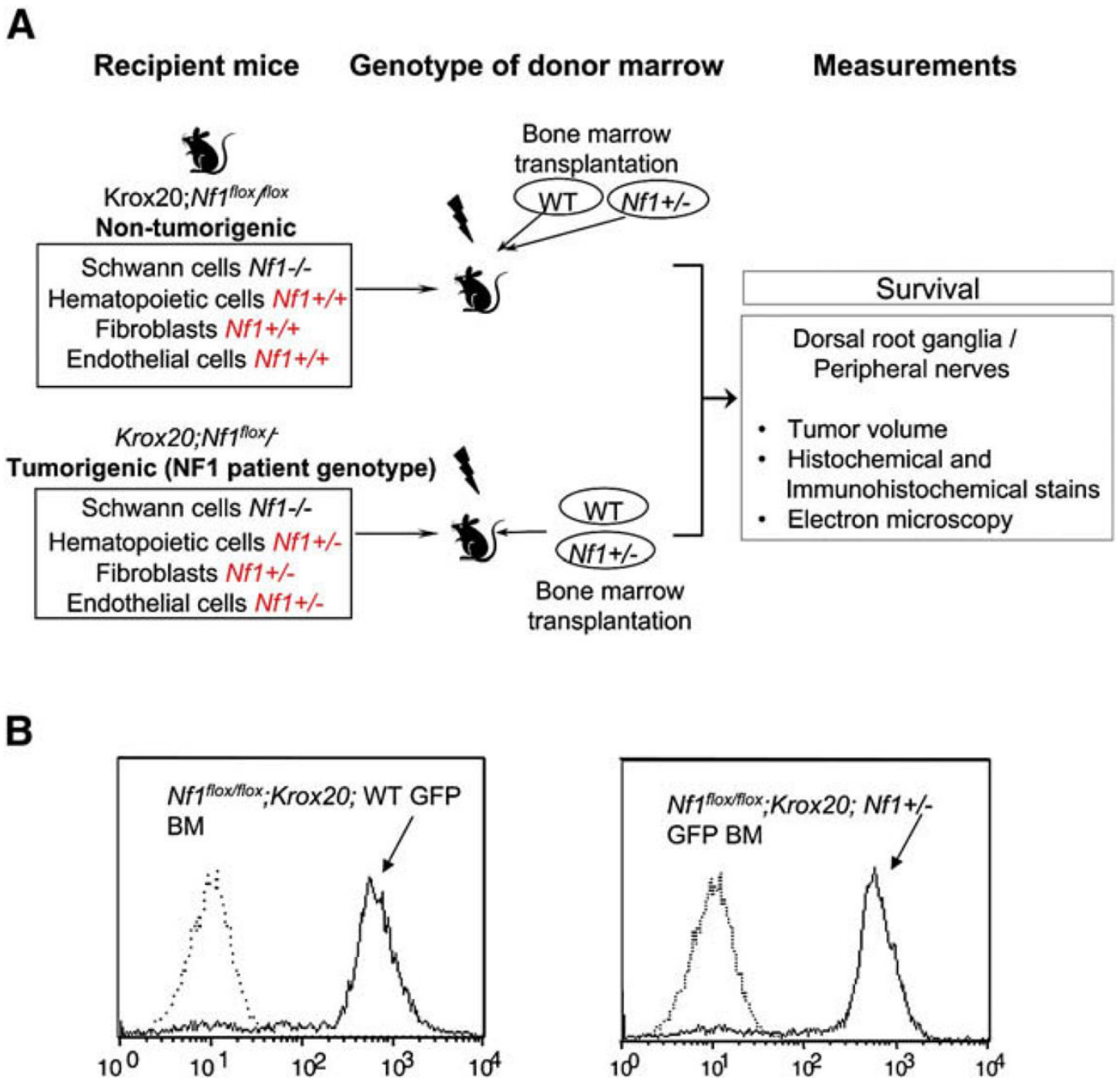

Figure 1. Strategy to Examine the Role of the Hematopoietic Microenvironment in Neurofibroma Formation

(A) Experimental design; schematic showing the genotypes of recipient mice, the genotypes of bone marrow cells following ionizing radiation of recipients, and measurements obtained following transplantation.

(B) Identification of donor bone marrow using fluorescence cytometry. Representative histograms of donor bone marrow cells isolated from previously irradiated Krox20;Nf1flox/flox recipients. The genotypes of transplanted cells are indicated. Dotted lines indicate the EGFP fluorescence intensity of bone marrow that lacks the EGFP transgene.

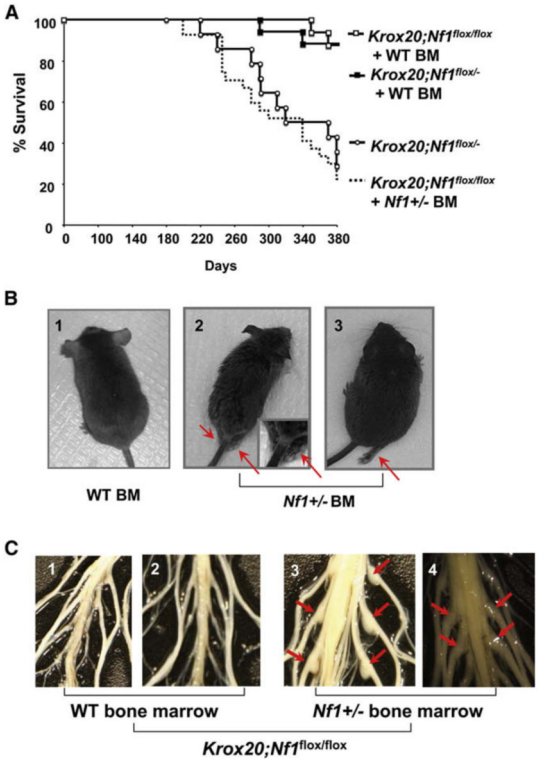

Figure 2. *Nf1*$^{+/-}$ Bone Marrow Is Necessary for Plexiform Neurofibroma Formation in *Krox20;Nf1*$^{flox/flox}$ and *Krox20;Nf1*$^{flox/-}$ Mice

(A) Previously irradiated *Krox20;Nf1*$^{flox/flox}$ and *Krox20;Nf1*$^{flox/-}$ mice transplanted with *Nf1*$^{+/-}$ or WT bone marrow were followed until 1 year of age. A Kaplan-Meier plot of percent survival (y axis) as a function of time (x axis) is shown. The genotypes are indicated. Comparisons of *Krox20;Nf1*$^{flox/flox}$+ *Nf1*$^{+/-}$ BM (dashed line) versus *Krox20;Nf1*$^{flox/flox}$+ WT BM (open squares) ($p < 0.002$); *Krox20;Nf1*$^{flox/flox}$+ *Nf1*$^{+/-}$ BM (dashed line) versus *Krox20;Nf1*$^{flox/-}$ (open circles) (no significant difference). *Krox20;Nf1*$^{flox/-}$ (open circles) versus *Krox20;Nf1*$^{flox/-}$ + WT bone marrow (closed squares) ($p < 0.0002$).

(B) Photographs of *Krox20;Nf1*$^{flox/flox}$ mice transplanted with WT BM (1) or *Nf1*$^{+/-}$ BM (2 and 3). Arrowheads identify limbs with motor paralysis.

(C) Dissections of dorsal root ganglia and peripheral nerves of *Krox20;Nf1*$^{flox/flox}$ mice transplanted with WT or *Nf1*$^{+/-}$ bone marrow. Arrowheads identify tumors in dorsal root ganglia and proximal peripheral nerves.

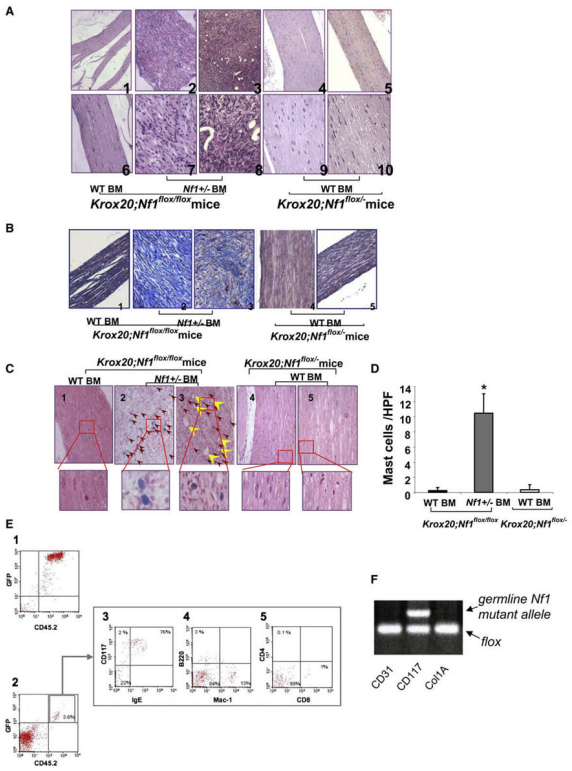

Figure 3. Tumors Isolated from *Krox20;Nf1*$^{flox/flox}$ Mice Transplanted with *Nf1*$^{+/-}$ Bone Marrow Have Histologic Features of Plexiform Neurofibromas

(A) Hematoxylin and eosin (H&E) sections of dorsal root ganglia and proximal peripheral nerves. Panels 1 and 6 are sections from a *Krox20;Nf1*$^{flox/flox}$ mouse transplanted with WT BM. Panels 2, 3, 7, and 8 are from *Krox20;Nf1*$^{flox/flox}$ mice transplanted with *Nf1*$^{+/-}$ BM. Panels 4, 5, 9, and 10 are from *Krox20;Nf1*$^{flox/-}$ mice transplanted with WT BM. Photos in upper panels were taken with a light microscope under 100x, whereas the lower panels were taken under 400x.

(B) 200x magnification of sections stained with Masson's trichrome. Genotypes of donor bone marrow and recipient mice are indicated.

(C) 200x magnification of sections stained with alcian blue. Red arrowheads identify mast cells. Yellow arrowheads identify blood vessels. High power magnification (1000x) insets of mast cells are indicated.

(D) Summary data indicating the number of mast cells scored within tumors or dorsal root ganglia (DRG) of *Krox20;Nf1*$^{flox/flox}$ and *Krox20;Nf1*$^{flox/-}$ recipients. Data represent the mean ± standard error of the mean (SEM) of five tumors or DRG per group. The genotypes of the donors and recipient mice are indicated. An asterisk indicates $p < 0.001$ significance of mast cells identified in recipients who received *Nf1*$^{+/-}$ versus WT bone marrow.

(E) Phenotypic evaluation of bone marrow-derived lineages using fluorescence cytometry. Bone marrow (panel 1) and tumor cells (panel 2) were isolated and sorted for EGFP+; CD45.2 positive populations. Tumor associated CD45.2 cells were then further separated to identify mast cell (panel 3), macrophage (panel 4), B-lymphocyte (panel 4), and T-lymphocyte populations (panel 5). The proportion of each hematopoietic cell population within the tumor is indicated.

(F) Genotyping of lineages isolated by FACS from tumors of *Krox20;Nf1*$^{flox/flox}$ mice transplanted with *Nf1*$^{+/-}$ BM. Arrows identify the amplified DNA products of the indicated alleles from the respective phenotypic lineages.

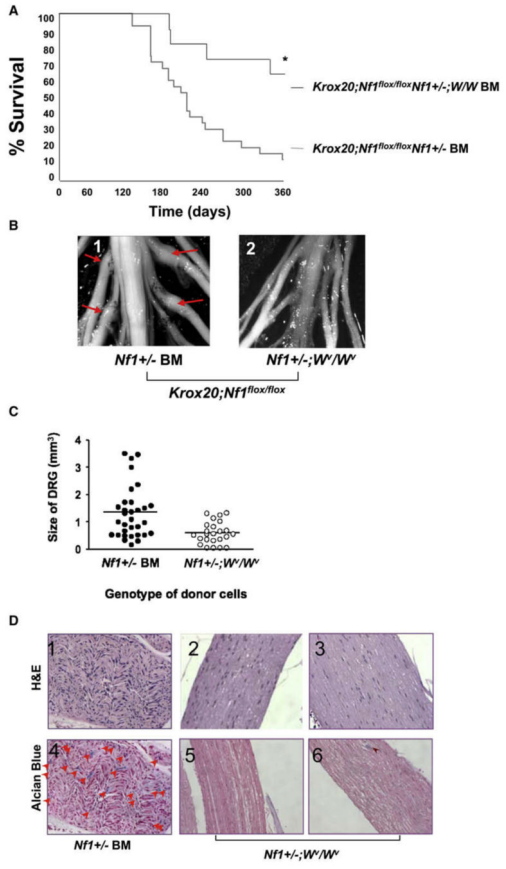

Figure 4. Genetic Disruption of c-kit in Adoptively Transferred *Nf1*$^{+/-}$ Bone Marrow Prevents the Genesis of Plexiform Neurofibromas in Recipient *Krox20;Nf1*$^{flox/flox}$ Mice

(A) *Krox20;Nf1*$^{flox/flox}$ mice were transplanted with *Nf1*$^{+/-}$ or *Nf1*$^{+/-}$;*W* mutant BM. A Kaplan-Meier plot of percent survival (y axis) as a function of time (x axis) is shown. The genotypes are indicated. An asterisk indicates $p < 0.002$ comparing survival of the two experimental groups.

(B) Photographs of the spinal cord and dorsal roots of *Krox20;Nf1*$^{flox/flox}$ mice transplanted with WT BM (panel 1) or *Nf1*$^{+/-}$ BM (panel 2). Arrows identify tumors in proximal nerves.

(C) Mean size of dorsal root ganglia (DRG) from the sciatic nerves of recipients transplanted with *Nf1*$^{+/-}$ or *Nf1*$^{+/-}$;*W/W* bone marrow. Each dot represents the size of an individual DRG. The line indicates the mean size of all DRG. An asterisk indicates $p < 0.01$ comparing size of DRG between two groups.

(D) Representative histologic sections of dorsal root ganglia and proximal spinal nerves of *Krox20;Nf1*$^{flox/flox}$ mice transplanted with *Nf1*$^{+/-}$ or *Nf1*$^{+/-}$;*W/W* mutant marrow. Panels 1–3 are sections stained with H&E; panels 4–6 are stained with alcian blue. Arrowheads indicate mast cells. The genotypes of donor bone marrow are indicated.

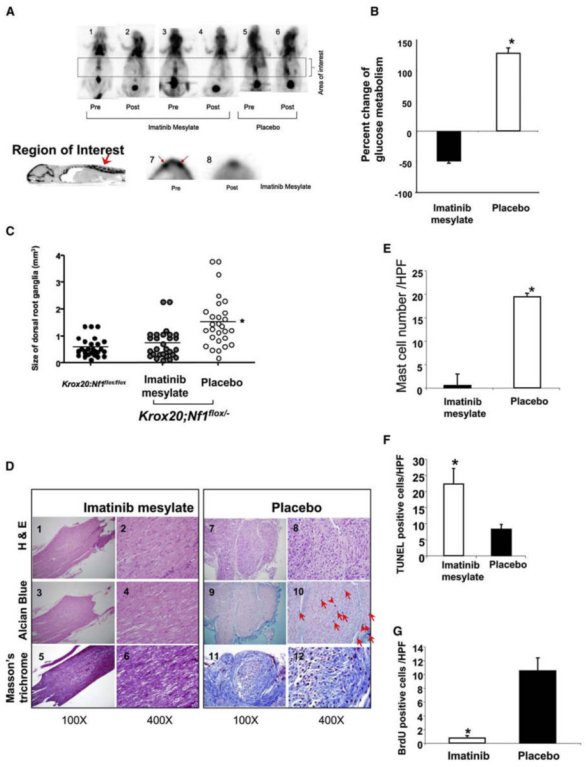

Figure 5. Treatment of *Krox20;Nf1*$^{flox/-}$ Mice with Imatinib Mesylate

(A) Change in mean FDG-PET-positive tumors after a 12 week treatment with imatinib mesylate. The temporal sequence of scans in three individual mice, and the experimental treatment groups are identified (panels1–6). A schematic identifying a high resolution region of interest and representative regions of interest prior and subsequent to treatment with imatinib mesylate are shown (panels 7 and 8). (B) Summary of changes in mean FDG-PET intensity after a 12 week treatment with imatinib mesylate or PBS. Data are presented as mean ± SEM. (C) Dissection of the peripheral nerves. Mean volume of dorsal root ganglia from all sciatic nerves of *Krox20;Nf1*$^{flox/-}$ mice treated with vehicle versus imatinib mesylate. The solid line indicates mean volume of each respective group. Each symbol indicates the volume of an individual nerve. *$p < 0.001$ comparing vehicle to imatinib mesylate. (D) Histological analysis of the *Krox20;Nf1*$^{flox/-}$ mice treated with imatinib mesylate or vehicle. Representative sections were shown following H&E staining, Alcian blue staining, and Masson's trichrome staining. The experimental therapy, the stains utilized to prepare the specimens, and the magnification are indicated. Red arrows identify mast cells found on the respective sections. (E) Imatinib mesylate reduces mast cell numbers in plexiform neurofibromas. Summary data of mast cells per 100× field of *Krox20;Nf1*$^{flox/-}$ mice treated with imatinib mesylate or vehicle. Data represent mean ± SEM of mast cells/ high power field from 10 fields of 12 tumors/DRG; an asterisk indicates $p < 0.01$ statistical difference between groups. (F and G) Imatinib mesylate induces apoptosis (F) and reduces proliferation (G) in plexiform neurofibromas. Summary data (mean ± SEM) of (F) apoptotic and (G) BrdU+ cells / high power field imatinib mesylate versus placebo; an asterisk indicates $p < 0.01$ statistical difference between groups.

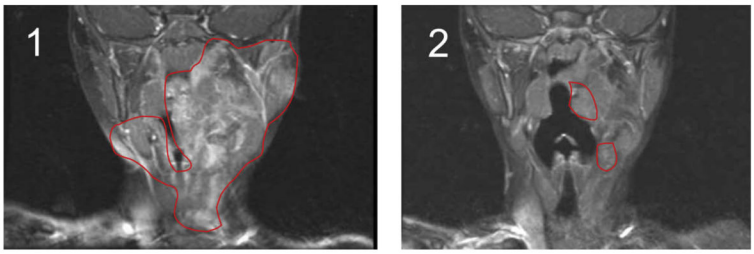

Figure 6. Evaluation of Imatinib Mesylate Efficacy in an Index Patient with a Plexiform Neurofibroma

Coronal MRI scans (T1 weighted images with gadolinium contrast and fat saturation) of the head and oropharynx of an NF1 patient with a plexiform neurofibroma before (panel 1) and 3 months following treatment with imatinib mesylate (panel 2). The region of the tumor in the respective images is indicated.